Robust H_∞ Attitude Stabilization for the Cluster Takeover of Non-cooperative Flexible Spacecraft

Xiaokui Yue, Ziyu Yang, Hongyu Yu, Panxing Huang, and Yuan Liu

Abstract In this paper, a cooperative control scheme based on the small spacecraft cluster is proposed for the takeover control of the failed flexible spacecraft in space. In order to overcome external disturbance, inertia uncertainty and controller gain perturbation, the controller spacecraft calculates the control torque which can stabilize the combined spacecraft in theory, and generates the desired control signal according to the robust H_∞ non-fragile control law set in advance. Based on the communication topology, the actuator spacecraft restores the control signal according to the distributed control torque allocation scheme considering the saturation state of all reaction wheels, and implements it to achieve the attitude stabilization and vibration suppression of the combined spacecraft. Simulation results show that the distributed control torque allocation scheme can implement the desired control signal with relatively small error. Under the condition that the external disturbance, controller gain perturbation and inertia uncertainty coexist, the angle and angular velocity of the combined spacecraft can be stabilized quickly. Moreover, the vibration of the flexible appendages can also be suppressed effectively. During the whole takeover control process, the dynamic allocation scheme can always ensure that all reaction wheels of each actuator spacecraft never reach saturation.

Keywords Cluster takeover · Attitude stabilization · Robust H_∞ · Non-fragile control · Control allocation

X. Yue (✉) · Z. Yang · H. Yu
National Key Laboratory of Aerospace Flight Dynamics, School of Astronautics, Northwestern Polytechnical University, Xi'an 710072, China
e-mail: xkyue@nwpu.edu.cn

P. Huang
Science and Technology on Space Intelligent Control Laboratory, Beijing Institute of Control Engineering, Beijing 100094, China

Y. Liu
Beijing Institute of Remote Sensing Information, Beijing 100011, China

S. Li (ed.), *Computational and Experimental Simulations in Engineering*, Mechanisms and Machine Science 146, https://doi.org/10.1007/978-3-031-44947-5_4

1 Introduction

The acquisition of non-cooperative spacecraft is the focus of research in recent years, which is mainly divided into two stages: pre-capture and post-capture [1]. The focus of the post-capture stage is how to realize the attitude and orbit takeover of the combination by the service spacecraft. As the disadvantages of large single integrated function spacecraft in taking over non-cooperative targets are gradually emerging, researchers tend to use modular spacecraft clusters to implement this mission [2]. Because the control force and torque provided by a single module spacecraft is limited, it is far from being able to meet the requirements of the control for the post-capture combination, which introduces the distribution of control torque. In addition, the input saturation problem is also different from the conventional spacecraft input saturation problem. In the control allocation, it is necessary to consider not only the overall control capability of the cluster, but also the reaction saturation of every single service spacecraft in the cluster.

In the current literature, the takeover of non-cooperative spacecraft has been widely discussed. Inertia unknown is the main parameter feature of the non-cooperative spacecraft, and the cost of high-precision parameter identification is very expensive, so inertia uncertainty is a problem that must be considered during the process of takeover mission [3]. Aiming at the inertia unknown problem of post-capture flexible spacecraft, an inertia-independent output feedback control strategy is designed in [4]. On the other hand, [5] uses the neural network to approach the unknown dynamic characteristics of the spacecraft and designs an event-triggered adaptive fuzzy controller which can overcome the inertia uncertainty. However, the input saturation is not explicitly considered in the above work. In the scenario where the multi-service spacecraft takes over the non-cooperative target, a distributed allocation strategy considering the angular momentum saturation of each reaction wheel of the service spacecraft is proposed in [6]. This strategy can always ensure that the allocation target can be satisfied and finally converge to the optimal allocation solution. On the basis of [7], an allocation strategy considering the maximum output torque of the service spacecraft is proposed in [8]. This scheme ensures that each service spacecraft will not be assigned control torque beyond its capability, but the allocation scheme cannot guarantee the allocation accuracy. In addition, an allocation scheme that does not rely on the iteration step size is proposed in [9] to make up for the shortcomings of the current allocation algorithm. Although the problem of input saturation in the process of control allocation has been properly dealt with, the saturation problem of the expected control torque has not been considered in the controller design. Moreover, because of the information transmission among multiple spacecraft, the perturbation of control signals has to be considered [10]. At present, the controller gain additive perturbation is the main problem discussed by researchers, but the control gain multiplicative perturbation is often ignored. In some cases, the multiplicative perturbation of the control gain will have a greater adverse impact on the performance of the control system [11]. Therefore, both types of controller gain perturbations need to be considered simultaneously.

Inspired by the above key issues and challenges, this paper captures the unknown and nonlinear terms as disturbances in the case of considering the inertia uncertainty of flexible spacecraft. On this basis, a robust H_∞ controller is designed considering both types of controller gain perturbation, and the conditions for explicit limiting of the desired control signal are given. Then the solution of controller gain is transformed into an optimization problem based on linear matrix inequalities. Finally, a distributed control torque allocation scheme is adopted, and the reasonable allocation is carried out considering the saturation of each reaction wheel of all the service spacecraft.

The text of this paper is as follows. In the second part, the dynamic model of flexible combination, the form of robust H_∞ controller, the relevant lemmas and assumptions required for controller design as well as the control objectives of this paper are given. The third part shows the main results of this paper, including the theorem of controller design and the control torque allocation scheme. The simulation results in the fourth part verify the effectiveness of the theory in this paper. The last part gives the conclusion.

2 Problem Formulation

2.1 Dynamics Modeling

The attitude control system of the post-capture flexible combination can be expressed as follows [12, 13]:

$$\begin{cases} \dot{\boldsymbol{x}}(t) = \left(\boldsymbol{A} + \Delta\boldsymbol{A}_p\right)\boldsymbol{x}(t) + \boldsymbol{B}_1\boldsymbol{u}(t) + \boldsymbol{B}_2\boldsymbol{w}(t) \\ \boldsymbol{y}(t) = \boldsymbol{C}\boldsymbol{x}(t) + \boldsymbol{v}(t) \end{cases} \tag{1}$$

where $\boldsymbol{x}(t) = \begin{bmatrix} \boldsymbol{\Theta}^{\mathrm{T}} & \boldsymbol{\omega}^{\mathrm{T}} & \boldsymbol{q}^{\mathrm{T}} & \tilde{\boldsymbol{\eta}}^{\mathrm{T}} \end{bmatrix}^{\mathrm{T}}$ is the defined state vector with $\boldsymbol{q} = \dot{\tilde{\boldsymbol{\eta}}} + \tilde{\boldsymbol{\Delta}}^{\mathrm{T}}\boldsymbol{\omega}$, $\boldsymbol{u}(t) = \boldsymbol{T}_c$ is the control input, and $\boldsymbol{y}(t)$ is the output vector with measurement error $\boldsymbol{v}(t)$; $\boldsymbol{w}(t) = \boldsymbol{w}_0(t) + \boldsymbol{B}_2^*(\Delta\boldsymbol{A}\boldsymbol{x}(t) + \Delta\boldsymbol{B}_1\boldsymbol{u}(t) + \Delta\boldsymbol{B}_2\boldsymbol{w}_0(t) + \boldsymbol{E}\boldsymbol{f}(t))$ is the constructed lumped disturbance capturing external disturbance $\boldsymbol{w}_0(t) = \boldsymbol{T}_d - \boldsymbol{\omega}^{\times}(\boldsymbol{J}_0\boldsymbol{\omega} + \tilde{\boldsymbol{\Delta}}\boldsymbol{q})$ with $\boldsymbol{T}_d$ denoting the external disturbance torque, inertia unknown matrices $\Delta\boldsymbol{A}$, $\Delta\boldsymbol{B}_2$ and actuator fault $\boldsymbol{E}\boldsymbol{f}(t)$. $\boldsymbol{B}_2^*$ denotes the pseudoinverse matrix of $\boldsymbol{B}_2$ and $\boldsymbol{E}$ denotes the distribution matrix of fault signal $\boldsymbol{f}(t)$. The related coefficient matrices in (1) are

$$\boldsymbol{A} = \begin{bmatrix} 0 & \boldsymbol{I} & 0 & 0 \\ 0 & -\boldsymbol{J}_{0n}^{-1}\tilde{\boldsymbol{\Delta}}\tilde{\boldsymbol{C}}\tilde{\boldsymbol{\Delta}}^{\mathrm{T}} & \boldsymbol{J}_{0n}^{-1}\tilde{\boldsymbol{\Delta}}\left(\tilde{\boldsymbol{C}} + \tilde{\boldsymbol{\Delta}}_p\boldsymbol{F}_2\right) & \boldsymbol{J}_{0n}^{-1}\tilde{\boldsymbol{\Delta}}\left(\tilde{\boldsymbol{K}} + \tilde{\boldsymbol{\Delta}}_p\boldsymbol{F}_1\right) \\ 0 & \tilde{\boldsymbol{C}}\tilde{\boldsymbol{\Delta}}^{\mathrm{T}} & -\left(\tilde{\boldsymbol{C}} + \tilde{\boldsymbol{\Delta}}_p\boldsymbol{F}_2\right) & -\left(\tilde{\boldsymbol{K}} + \tilde{\boldsymbol{\Delta}}_p\boldsymbol{F}_1\right) \\ 0 & -\tilde{\boldsymbol{\Delta}}^{\mathrm{T}} & \boldsymbol{I} & 0 \end{bmatrix},$$

$$\boldsymbol{B}_1 = \boldsymbol{B}_2 = \begin{bmatrix} 0 \\ \boldsymbol{J}_{0n}^{-1} \\ 0 \\ 0 \end{bmatrix}, \ \boldsymbol{C} = \boldsymbol{I}.$$

The matrices containing unknown inertia are

$$\begin{aligned} \Delta \boldsymbol{A} &= \boldsymbol{A}(\boldsymbol{J}) - \boldsymbol{A}(\boldsymbol{J}_n) \\ &= \begin{bmatrix} 0 & 0 & 0 & 0 \\ 0 & \left(\boldsymbol{J}_{0n}^{-1} - \boldsymbol{J}_0^{-1}\right)\tilde{\boldsymbol{\Delta}}\tilde{\boldsymbol{C}}\tilde{\boldsymbol{\Delta}}^{\mathrm{T}} & \left(\boldsymbol{J}_0^{-1} - \boldsymbol{J}_{0n}^{-1}\right)\tilde{\boldsymbol{\Delta}}\left(\tilde{\boldsymbol{C}} + \tilde{\boldsymbol{\Delta}}_p \boldsymbol{F}_b\right) & \left(\boldsymbol{J}_0^{-1} - \boldsymbol{J}_{0n}^{-1}\right)\tilde{\boldsymbol{\Delta}}\left(\tilde{\boldsymbol{K}} + \tilde{\boldsymbol{\Delta}}_p \boldsymbol{F}_a\right) \\ 0 & 0 & 0 & 0 \\ 0 & 0 & 0 & 0 \end{bmatrix}, \end{aligned}$$

$$\begin{aligned} \Delta \boldsymbol{B}_1 = \Delta \boldsymbol{B}_2 &= \boldsymbol{B}_1(\boldsymbol{J}) - \boldsymbol{B}_1(\boldsymbol{J}_n) \\ &= \begin{bmatrix} 0 \\ \boldsymbol{J}_0^{-1} - \boldsymbol{J}_{0n}^{-1} \\ 0 \\ 0 \end{bmatrix} \end{aligned}$$

in which $\boldsymbol{J}$ is the inertia matrix; $\boldsymbol{\omega} = \begin{bmatrix} \omega_x & \omega_y & \omega_z \end{bmatrix}^{\mathrm{T}}$ represents the angular velocity vector; $\tilde{\boldsymbol{\Delta}} \in \mathbb{R}^{3\times k}$ is the rigid-flexible coupling matrix, and k is the order of flexible modes; $\tilde{\boldsymbol{\eta}} \in \mathbb{R}^k$ is the modal displacement; $\tilde{\boldsymbol{C}} = \mathrm{diag}\left\{\begin{bmatrix} 2\tilde{\xi}_1\Omega_1 & 2\tilde{\xi}_2\Omega_2 & \cdots & 2\tilde{\xi}_k\Omega_k \end{bmatrix}\right\}$ is the modal damping matrix; Ω_i $(i = 1, 2, \ldots, k)$ and $\tilde{\xi}_i$ denote the natural frequencies and damping ratios respectively; $u_p = \boldsymbol{F}_1\tilde{\boldsymbol{\eta}} + \boldsymbol{F}_2\boldsymbol{q}$ is the piezoelectric input with the feedback coefficients $\boldsymbol{F}_1$ and $\boldsymbol{F}_2$ of the piezoelectric actuators, working through the coupling matrix $\tilde{\boldsymbol{\Delta}}_p$ to help suppress vibration; $\tilde{\boldsymbol{K}} = \mathrm{diag}\left\{\begin{bmatrix} \Omega_1^2 & \Omega_2^2 & \cdots & \Omega_k^2 \end{bmatrix}\right\}$ is the stiffness matrix. In addition, $\boldsymbol{J}_{0n} = \boldsymbol{J}_n - \tilde{\boldsymbol{\Delta}}\tilde{\boldsymbol{\Delta}}^{\mathrm{T}}$ with $\boldsymbol{J}_0 = \boldsymbol{J} - \tilde{\boldsymbol{\Delta}}\tilde{\boldsymbol{\Delta}}^{\mathrm{T}}$, and $\boldsymbol{J}_n$ denotes the introduced the nominal inertia matrix.

$\boldsymbol{\Delta A}_p$ is the model parameter uncertainty expressed as

$$\boldsymbol{\Delta A}_p(t) = \boldsymbol{M}\boldsymbol{F}(t)\boldsymbol{N}, \ \|\boldsymbol{F}(t)\| \leq 1, \quad \forall t \tag{2}$$

where $\boldsymbol{M}$ and $\boldsymbol{N}$ are known real matrices, and $\boldsymbol{F}(t)$ is the Lebesgue function matrix [14].

Different from the previous non-fragile controllers, a more general hybrid non-fragile state feedback controller is adopted in this paper:

$$\boldsymbol{u}(t) = (\boldsymbol{K} + \overline{\rho}(\Delta \boldsymbol{K}_a + \Delta \boldsymbol{K}_m))\boldsymbol{x}(t) \tag{3}$$

where $\boldsymbol{K}$ is the controller gain matrix, and $\overline{\rho}$ represents the mean of the probability of random occurrence of controller gain perturbation. $\Delta \boldsymbol{K}_a$ and $\Delta \boldsymbol{K}_m$ represent two types of controller gain perturbation and have the following forms respectively:

$$\Delta \boldsymbol{K}_a(t) = \boldsymbol{M}_a \boldsymbol{F}_a(t) \boldsymbol{N}_a, \ \|\boldsymbol{F}_a(t)\| \leq 1, \quad \forall t \tag{4}$$

$$\Delta \boldsymbol{K}_m(t) = \boldsymbol{M}_m \boldsymbol{F}_m(t) \boldsymbol{N}_m \boldsymbol{K}, \ \|\boldsymbol{F}_m(t)\| \leq 1, \quad \forall t \tag{5}$$

The definitions of $\boldsymbol{M}_a, \boldsymbol{N}_a, \boldsymbol{F}_a(t), \boldsymbol{M}_m, \boldsymbol{N}_m$ and $\boldsymbol{F}_m(t)$ are similar to those in (2).

It is worth mentioning that the input constraint problem in this paper is described by the following formula:

$$\|\boldsymbol{u}(t)\| \leq \lambda \tag{6}$$

where $\lambda = \sqrt{\lambda_0}$ denotes the maximum value of 2 norm of control input and $\lambda_0 > 0$.

Substitute the controller (3) into the system (1), and one has

$$\begin{cases} \dot{\boldsymbol{x}}(t) = \big(\boldsymbol{A} + \Delta \boldsymbol{A}_p + \boldsymbol{B}_1 \boldsymbol{K} + \overline{\rho} \boldsymbol{B}_1 (\Delta \boldsymbol{K}_a + \Delta \boldsymbol{K}_m)\big) \boldsymbol{x}(t) + \boldsymbol{B}_1 \boldsymbol{w}(t) \\ \boldsymbol{y}(t) = \boldsymbol{C} \boldsymbol{x}(t) + \boldsymbol{v}(t) \end{cases} \tag{7}$$

2.2 Preliminaries

Before giving the main results of the required solution, some necessary assumptions and lemmas need to be given first.

Assumption 1 $\boldsymbol{w}(t)$ is piecewise bounded and continuous, and $\boldsymbol{v}(t) \in L_2[0, \infty]$.

Remark 1 The disturbance and uncertainty are bounded, which is one of the basic assumptions in robust control. The piecewise boundedness and continuity of the lumped disturbance have been proved in [15]. Moreover, the controller design in this paper does not need the norm bound of $\boldsymbol{w}(t)$ and $\boldsymbol{v}(t)$ [16].

Lemma 1 (Schur Complement Lemma [17]). *The equivalent condition of a negative definite block symmetric matrix* $\boldsymbol{\Theta} = \begin{bmatrix} \boldsymbol{\Theta}_{11} & \boldsymbol{\Theta}_{12} \\ * & \boldsymbol{\Theta}_{22} \end{bmatrix}$ *are*

(1) $\boldsymbol{\Theta} < 0$; (2) $\boldsymbol{\Theta}_{11} < 0, \boldsymbol{\Theta}_{22} - \boldsymbol{\Theta}_{12}^{\mathrm{T}} \boldsymbol{\Theta}_{11}^{-1} \boldsymbol{\Theta}_{12} < 0$; (3) $\boldsymbol{\Theta}_{22} < 0, \boldsymbol{\Theta}_{11} - \boldsymbol{\Theta}_{12} \boldsymbol{\Theta}_{22}^{-1} \boldsymbol{\Theta}_{12}^{\mathrm{T}} < 0$.

Lemma 2 [18] *For matrices* $\hat{\boldsymbol{M}}$, $\hat{\boldsymbol{N}}$ *and* $\hat{\boldsymbol{F}}(t)$ *with matching dimensions, and* $\left\|\hat{\boldsymbol{F}}(\mathrm{t})\right\| \leq 1$, *then* $\hat{\boldsymbol{M}} \hat{\boldsymbol{F}}(t) \hat{\boldsymbol{N}} + \hat{\boldsymbol{N}}^{\mathrm{T}} \hat{\boldsymbol{F}}^{\mathrm{T}}(t) \hat{\boldsymbol{M}}^{\mathrm{T}} \leq \hat{\xi}^{-1} \hat{\boldsymbol{M}} \hat{\boldsymbol{M}}^{\mathrm{T}} + \hat{\xi} \hat{\boldsymbol{N}}^{\mathrm{T}} \hat{\boldsymbol{N}}$ *will hold for any scalar* $\hat{\xi} > 0$.

Lemma 3 [11] *Provided matrices $\tilde{\boldsymbol{M}}$ and $\tilde{\boldsymbol{N}}$ have appropriate dimensions, then for all $\tilde{\varepsilon} > 0$, the following inequality will hold*

$$\begin{bmatrix} 0 & \tilde{\boldsymbol{N}}\tilde{\boldsymbol{M}}^{\boldsymbol{T}} \\ * & 0 \end{bmatrix} \leq \begin{bmatrix} \tilde{\varepsilon}\tilde{\boldsymbol{N}}\tilde{\boldsymbol{N}}^{\boldsymbol{T}} & 0 \\ * & \varepsilon^{-1}\tilde{\boldsymbol{M}}\tilde{\boldsymbol{M}}^{\boldsymbol{T}} \end{bmatrix}$$

Lemma 4 [11, 15] *Suppose that there exist symmetric positive definite matrix $\boldsymbol{X}$, matrix $\boldsymbol{W}$ and scalars λ_0, γ_0, ε and η_0 satisfying inequalities (8)–(9), then the control input constraint expressed by Eq. (6) is satisfied.*

$$\begin{bmatrix} -\boldsymbol{X} & \boldsymbol{W}^{\mathrm{T}} & \boldsymbol{X}^{\mathrm{T}} \\ * & -\lambda_0\gamma_0^{-1}\boldsymbol{I} + \varepsilon^{-1}\overline{\rho}^2\eta_0^2\boldsymbol{I} & 0 \\ * & * & -\varepsilon^{-1}\boldsymbol{I} \end{bmatrix} < 0 \tag{8}$$

$$\begin{bmatrix} -\gamma_0 & \boldsymbol{x}^{\mathrm{T}}(0) \\ * & -\boldsymbol{X} \end{bmatrix} < 0 \tag{9}$$

where $\boldsymbol{W} = \boldsymbol{K}\boldsymbol{X}$ with $\boldsymbol{K}$ denoting the controller gain matrix, $\boldsymbol{x}(0)$ is the initial state of the system, $\|\Delta\boldsymbol{K}_a + \Delta\boldsymbol{K}_m\| < \eta_0$, and $\boldsymbol{x}^{\mathrm{T}}(0)\boldsymbol{P}\boldsymbol{x}(0) \leq \gamma_0$ with $\boldsymbol{P}$ denoting the Lyapunov matrix in the Lyapunov function.

2.3 Control Objectives

1. When $\boldsymbol{w}(t) = 0$ and $\boldsymbol{v}(t) = 0$, the closed-loop attitude stabilization system (7) is quadratically stable.
2. For a given scalar $\gamma > 0$, $\boldsymbol{G}_{\hat{w}y}(s)$ is the transfer function from $\hat{\boldsymbol{w}}(t)$ to $\boldsymbol{y}(t)$, where $\hat{\boldsymbol{w}}(t) = 0$ and $\left\|\boldsymbol{G}_{\hat{w}y}(s)\right\|_\infty < \gamma$ should be satisfied.
3. The control input satisfies inequality (6).

3 Main Results

3.1 Robust $\mathbf{H}_\infty$ Controller Design

This section presents a robust H_∞ controller scheme for small cluster spacecraft, which can output the control signal that can stabilize the system (1) on the premise of satisfying the input saturation condition (6). The following theorem will give the calculation of the desired control signal.

Theorem 1 *When two perturbations of controller gain coexist, if there are positive definite symmetric matrix* $\boldsymbol{P}$ *and matrix* $\boldsymbol{W}$*, such that linear matrix inequalities (9)–(10) hold, then the system (7) can be quadratically stable under the action of the controller (3), the output* $\boldsymbol{y}(t)$ *satisfies the* H_∞ *performance constraint and the desired control signal* $\boldsymbol{u}(t)$ *satisfies the input saturation condition.*

$$\begin{bmatrix} \boldsymbol{\Xi}_{11} & \boldsymbol{\Xi}_{12} \\ * & \boldsymbol{\Xi}_{22} \end{bmatrix} < 0 \tag{10}$$

where

$$\boldsymbol{\Xi}_{11} = \boldsymbol{A}\boldsymbol{X} + \boldsymbol{X}\boldsymbol{A}^T + \boldsymbol{B}_1\boldsymbol{W} + \boldsymbol{W}^{\mathrm{T}}\boldsymbol{B}_1^{\mathrm{T}}$$

$$\boldsymbol{\Xi}_{12} = \begin{bmatrix} \boldsymbol{B}_2 & \boldsymbol{X}\boldsymbol{C}^{\mathrm{T}} & \boldsymbol{M} & \boldsymbol{X}\boldsymbol{N}^{\mathrm{T}} & \boldsymbol{B}_1\boldsymbol{M}_a & \boldsymbol{X}\boldsymbol{N}_a^{\mathrm{T}} & \boldsymbol{B}_1\boldsymbol{M}_m & \boldsymbol{X}\boldsymbol{K}^{\mathrm{T}}\boldsymbol{N}_m^{\mathrm{T}} & \boldsymbol{X}\boldsymbol{C}^{\mathrm{T}} \end{bmatrix}^{\mathrm{T}}$$

$$\begin{aligned} \boldsymbol{\Xi}_{22} = \mathrm{diag}\big(\big[& -\hat{\gamma}\boldsymbol{I} - \big(1-\hat{\gamma}\big)\boldsymbol{I} - \xi^{-1}\boldsymbol{I} - \xi\boldsymbol{I} - (\bar{\rho}\xi_a)^{-1}\boldsymbol{I} \\ & - \bar{\rho}^{-1}\xi_a\boldsymbol{I} - (\bar{\rho}\xi_m)^{-1}\boldsymbol{I} - \bar{\rho}^{-1}\xi_m\boldsymbol{I} - \boldsymbol{I}\big]\big) \end{aligned}$$

Under the constraints of (9)–(10), $\hat{\gamma} = \gamma^2$ *is minimized to find feasible solutions, and the controller gain is obtained by* $\boldsymbol{K} = \boldsymbol{W}\boldsymbol{X}^{-1}$.

Proof First, the quadratic stability of the system is proved when $\boldsymbol{w}(t) = 0$ and $\boldsymbol{v}(t) = 0$. Choose the following Lyapunov function

$$\boldsymbol{V}(t) = \boldsymbol{x}(t)\boldsymbol{P}\boldsymbol{x}^{\mathrm{T}}(t)$$

where $\boldsymbol{P} = \boldsymbol{X}^{-1}$. Then, the derivative of $\boldsymbol{V}(t)$ with respect to time is

$$\begin{aligned} \dot{\boldsymbol{V}}(t) &= \dot{\boldsymbol{x}}^{\mathrm{T}}(t)\boldsymbol{P}\boldsymbol{x}(t) + \boldsymbol{x}^{\mathrm{T}}(t)\boldsymbol{P}\dot{\boldsymbol{x}}(t) \\ &= \boldsymbol{x}^{\mathrm{T}}(t)\Big[\big(\boldsymbol{A} + \boldsymbol{\Delta}\boldsymbol{A}_p + \boldsymbol{B}_1\boldsymbol{K} + \overline{\rho}\boldsymbol{B}_1(\Delta\boldsymbol{K}_a + \Delta\boldsymbol{K}_m)\big)^{\mathrm{T}}\boldsymbol{P} \\ &\quad + \boldsymbol{P}\big(\boldsymbol{A} + \boldsymbol{\Delta}\boldsymbol{A}_p + \boldsymbol{B}_1\boldsymbol{K} + \overline{\rho}\boldsymbol{B}_1(\Delta\boldsymbol{K}_a + \Delta\boldsymbol{K}_m)\big)\Big]\boldsymbol{x}(t) \\ &= \boldsymbol{x}^{\mathrm{T}}(t)\big[(\boldsymbol{A} + \boldsymbol{B}_1\boldsymbol{K})^{\mathrm{T}}\boldsymbol{P} + \boldsymbol{P}(\boldsymbol{A} + \boldsymbol{B}_1\boldsymbol{K})\big]\boldsymbol{x}(t) \\ &\quad + \boldsymbol{x}^{\mathrm{T}}(t)\boldsymbol{P}\boldsymbol{M}\boldsymbol{F}(t)\boldsymbol{N}\boldsymbol{x}(t) + \boldsymbol{x}^{\mathrm{T}}(t)\boldsymbol{N}^{\mathrm{T}}\boldsymbol{F}^{\mathrm{T}}(t)\boldsymbol{M}^{\mathrm{T}}\boldsymbol{P}\boldsymbol{x}(t) \\ &\quad + \overline{\rho}\boldsymbol{x}^{\mathrm{T}}(t)\boldsymbol{P}\boldsymbol{B}_1\boldsymbol{M}_a\boldsymbol{F}_a(t)\boldsymbol{N}_a\boldsymbol{x}(t) + \overline{\rho}\boldsymbol{x}^{\mathrm{T}}(t)\boldsymbol{N}_a^{\mathrm{T}}\boldsymbol{F}_a^{\mathrm{T}}(t)\boldsymbol{M}_a^{\mathrm{T}}\boldsymbol{B}_1^{\mathrm{T}}\boldsymbol{P}\boldsymbol{x}(t) \\ &\quad + \overline{\rho}\boldsymbol{x}^{\mathrm{T}}(t)\boldsymbol{P}\boldsymbol{B}_1\boldsymbol{M}_m\boldsymbol{F}_m(t)\boldsymbol{N}_m\boldsymbol{K}\boldsymbol{x}(t) + \overline{\rho}\boldsymbol{x}^{\mathrm{T}}(t)\boldsymbol{K}^{\mathrm{T}}\boldsymbol{N}_m^{\mathrm{T}}\boldsymbol{F}_m^{\mathrm{T}}(t)\boldsymbol{M}_m^{\mathrm{T}}\boldsymbol{B}_m^{\mathrm{T}}\boldsymbol{P}\boldsymbol{x}(t) \\ &= \boldsymbol{x}^{\mathrm{T}}(t)\big[(\boldsymbol{A} + \boldsymbol{B}_1\boldsymbol{K})^{\mathrm{T}}\boldsymbol{P} + \boldsymbol{P}(\boldsymbol{A} + \boldsymbol{B}_1\boldsymbol{K})\big]\boldsymbol{x}(t) + 2\boldsymbol{x}^{\mathrm{T}}(t)\boldsymbol{P}\boldsymbol{M}\boldsymbol{F}(t)\boldsymbol{N}\boldsymbol{x}(t) \\ &\quad + 2\overline{\rho}\boldsymbol{x}^{\mathrm{T}}(t)\boldsymbol{P}\boldsymbol{B}_1\boldsymbol{M}_a\boldsymbol{F}_a(t)\boldsymbol{N}_a\boldsymbol{x}(t) + 2\overline{\rho}\boldsymbol{x}^{\mathrm{T}}(t)\boldsymbol{P}\boldsymbol{B}_1\boldsymbol{M}_m\boldsymbol{F}_m(t)\boldsymbol{N}_m\boldsymbol{x}(t) \\ &\le \boldsymbol{x}^{\mathrm{T}}(t)\,\boldsymbol{Q}_0\boldsymbol{x}(t) \end{aligned}$$

where $\boldsymbol{Q}_0 = (\boldsymbol{A}+\boldsymbol{B}_1\boldsymbol{K})^{\mathrm{T}}\boldsymbol{P} + \boldsymbol{P}(\boldsymbol{A}+\boldsymbol{B}_1\boldsymbol{K}) + \xi\boldsymbol{P}\boldsymbol{M}\boldsymbol{M}^{\mathrm{T}}\boldsymbol{P} + \xi^{-1}\boldsymbol{N}^{\mathrm{T}}\boldsymbol{N} + \xi_a\overline{\rho}\boldsymbol{P}\boldsymbol{B}_1\boldsymbol{M}_a\boldsymbol{M}_a^{\mathrm{T}}\boldsymbol{B}_1^{\mathrm{T}}\boldsymbol{P} + \xi_a^{-1}\overline{\rho}\boldsymbol{N}_a^{\mathrm{T}}\boldsymbol{N}_a + \xi_m\overline{\rho}\boldsymbol{P}\boldsymbol{B}_1\boldsymbol{M}_m\boldsymbol{M}_m^{\mathrm{T}}\boldsymbol{B}_1^{\mathrm{T}}\boldsymbol{P} + \xi_m^{-1}\overline{\rho}\boldsymbol{K}^{\mathrm{T}}\boldsymbol{N}_m^{\mathrm{T}}\boldsymbol{N}_m\boldsymbol{K}$

Based on the above, if $\boldsymbol{Q}_0 < 0$, one has $\dot{\boldsymbol{V}}(t) \le 0$ and

$$\dot{\boldsymbol{V}}(t) \le \boldsymbol{x}^{\mathrm{T}}(t)\,\boldsymbol{Q}_0\boldsymbol{x}(t) \le \lambda_{\max}(\boldsymbol{Q}_0)\boldsymbol{x}^{\mathrm{T}}(t)\boldsymbol{x}(t)$$

Choose $\alpha = -\lambda_{\max}(\boldsymbol{Q}_0) > 0$, one has

$$\dot{\boldsymbol{V}}(t) \le -\alpha\|\boldsymbol{x}(t)\|_2^2$$

Thus, when $\boldsymbol{w}(t) = 0$ and $\boldsymbol{v}(t) = 0$, the closed-loop attitude stabilization system (7) is quadratically stable.

Consider the following functional

$$J = \int_0^\infty \Big[\boldsymbol{y}(t)^{\mathrm{T}}\boldsymbol{y}(t) - \gamma^2\hat{\boldsymbol{w}}^{\mathrm{T}}(t)\hat{\boldsymbol{w}}(t)\Big]dt$$

Because of the quadratic stability, for any $\hat{\boldsymbol{w}}(t) \ne 0 \in L_2[0,\infty)$, under zero initial condition, it can be obtained that

$$\begin{aligned}
J &= \int_0^\infty \big[\boldsymbol{y}(t)^{\mathrm{T}}\boldsymbol{y}(t) - \gamma^2\hat{\boldsymbol{w}}(t)^{\mathrm{T}}\hat{\boldsymbol{w}}(t) + \dot{\boldsymbol{V}}(t)\big]dt - \boldsymbol{V}(\infty) + \boldsymbol{V}(0) \\
&= \int_0^\infty \Big[\boldsymbol{x}(t)^{\mathrm{T}}\hat{\boldsymbol{C}}^{\mathrm{T}}\hat{\boldsymbol{C}}\boldsymbol{x}(t) + 2\boldsymbol{x}(t)^{\mathrm{T}}\hat{\boldsymbol{C}}^{\mathrm{T}}\boldsymbol{v}(t) + \boldsymbol{v}(t)^{\mathrm{T}}\boldsymbol{v}(t) \\
&\quad - \gamma^2\big(\boldsymbol{w}(t)^{\mathrm{T}}\boldsymbol{w}(t) + \boldsymbol{v}(t)^{\mathrm{T}}\boldsymbol{v}(t)\big) + \boldsymbol{x}(t)^{\mathrm{T}}\boldsymbol{Q}_0\boldsymbol{x}(t) + 2\boldsymbol{x}(t)^{\mathrm{T}}\boldsymbol{P}\boldsymbol{B}_2\boldsymbol{w}(t)\Big]dt \\
&\le \int_0^\infty \begin{bmatrix}\boldsymbol{x}(t)^{\mathrm{T}} & \boldsymbol{w}(t)^{\mathrm{T}} & \boldsymbol{v}(t)^{\mathrm{T}}\end{bmatrix}\begin{bmatrix}\boldsymbol{Q}_0 + \boldsymbol{C}^{\mathrm{T}}\boldsymbol{C} & \boldsymbol{P}\boldsymbol{B}_2 & \boldsymbol{C}^{\mathrm{T}} \\ * & -\gamma^2\boldsymbol{I} & 0 \\ * & * & (1-\gamma^2)\boldsymbol{I}\end{bmatrix}\begin{bmatrix}\boldsymbol{x}(t) \\ \boldsymbol{w}(t) \\ \boldsymbol{v}(t)\end{bmatrix}dt
\end{aligned}$$

It is easy to know when the following inequality holds, $J < 0$.

$$\begin{bmatrix}\boldsymbol{Q}_0 + \boldsymbol{C}^{\mathrm{T}}\boldsymbol{C} & \boldsymbol{P}\boldsymbol{B}_2 & \boldsymbol{C}^{\mathrm{T}} \\ * & -\gamma^2\boldsymbol{I} & 0 \\ * & * & \big(1-\gamma^2\big)\boldsymbol{I}\end{bmatrix} < 0 \tag{11}$$

According to Lemma 1, (11) is equivalent to

$$\begin{bmatrix}
(\boldsymbol{A}+\boldsymbol{B}_1\boldsymbol{K})\boldsymbol{P}+\boldsymbol{P}(\boldsymbol{A}+\boldsymbol{B}_1\boldsymbol{K})^{\mathrm{T}} & \boldsymbol{P}\boldsymbol{B}_2 & \boldsymbol{C}^{\mathrm{T}} & \boldsymbol{P}\boldsymbol{M} & \boldsymbol{N}^{\mathrm{T}} \\
* & -\gamma^2\boldsymbol{I} & 0 & 0 & 0 \\
* & * & -\left(1-\gamma^2\right)\boldsymbol{I} & 0 & 0 \\
* & * & * & -\xi^{-1}\boldsymbol{I} & 0 \\
* & * & * & * & -\xi\boldsymbol{I} \\
* & * & * & * & * \\
* & * & * & * & * \\
* & * & * & * & * \\
* & * & * & * & * \\
* & * & * & * & *
\end{bmatrix}$$

$$\begin{bmatrix}
\boldsymbol{P}\boldsymbol{B}_1\boldsymbol{M}_a & \boldsymbol{N}_a^{\mathrm{T}} & \boldsymbol{P}\boldsymbol{B}_1\boldsymbol{M}_m & \boldsymbol{K}^{\mathrm{T}}\boldsymbol{N}_m^{\mathrm{T}} & \boldsymbol{C}^{\mathrm{T}} \\
0 & 0 & 0 & 0 & 0 \\
0 & 0 & 0 & 0 & 0 \\
0 & 0 & 0 & 0 & 0 \\
0 & 0 & 0 & 0 & 0 \\
-(\bar{\rho}\xi_a)^{-1}\boldsymbol{I} & 0 & 0 & 0 & 0 \\
* & -\bar{\rho}^{-1}\xi_a\boldsymbol{I} & 0 & 0 & 0 \\
* & * & -(\bar{\rho}\xi_m)^{-1}\boldsymbol{I} & 0 & 0 \\
* & * & * & -\bar{\rho}^{-1}\xi_m\boldsymbol{I} & 0 \\
* & * & * & * & -\boldsymbol{I}
\end{bmatrix} < 0 \tag{12}$$

Multiplying both sides of Inequality (12) by $\mathrm{diag}\left(\left[\boldsymbol{P}^{-1},\boldsymbol{I},\boldsymbol{I},\boldsymbol{I},\boldsymbol{I},\boldsymbol{I},\boldsymbol{I},\boldsymbol{I},\boldsymbol{I},\boldsymbol{I}\right]\right)$, and choosing $\boldsymbol{P}^{-1}=\boldsymbol{X}$, one has

$$\begin{bmatrix}
\boldsymbol{A}\boldsymbol{X}+\boldsymbol{X}\boldsymbol{A}^{\mathrm{T}}+\boldsymbol{B}_1\boldsymbol{K}\boldsymbol{X}+\boldsymbol{X}\boldsymbol{B}_1^{\mathrm{T}}\boldsymbol{K}^{\mathrm{T}} & \boldsymbol{B}_2 & \boldsymbol{X}\boldsymbol{C}^{\mathrm{T}} & \boldsymbol{M} & \boldsymbol{X}\boldsymbol{N}^{\mathrm{T}} \\
* & -\gamma^2\boldsymbol{I} & 0 & 0 & 0 \\
* & * & -\left(1-\gamma^2\right)\boldsymbol{I} & 0 & 0 \\
* & * & * & -\xi^{-1}\boldsymbol{I} & 0 \\
* & * & * & * & -\xi\boldsymbol{I} \\
* & * & * & * & * \\
* & * & * & * & * \\
* & * & * & * & * \\
* & * & * & * & * \\
* & * & * & * & *
\end{bmatrix}$$

$$\begin{bmatrix} \boldsymbol{B}_1\boldsymbol{M}_a & \boldsymbol{X}\boldsymbol{N}_a^{\mathrm{T}} & \boldsymbol{B}_1\boldsymbol{M}_m & \boldsymbol{X}\boldsymbol{K}^{\mathrm{T}}\boldsymbol{N}_m^{\mathrm{T}} & \boldsymbol{X}\boldsymbol{C}^{\mathrm{T}} \\ 0 & 0 & 0 & 0 & 0 \\ 0 & 0 & 0 & 0 & 0 \\ 0 & 0 & 0 & 0 & 0 \\ 0 & 0 & 0 & 0 & 0 \\ -(\bar{\rho}\xi_a)^{-1}\boldsymbol{I} & 0 & 0 & 0 & 0 \\ * & -\bar{\rho}^{-1}\xi_a\boldsymbol{I} & 0 & 0 & 0 \\ * & * & -(\bar{\rho}\xi_m)^{-1}\boldsymbol{I} & 0 & 0 \\ * & * & * & -\bar{\rho}^{-1}\xi_m\boldsymbol{I} & 0 \\ * & * & * & * & -\boldsymbol{I} \end{bmatrix} < 0 \tag{13}$$

Substitute $\boldsymbol{W} = \boldsymbol{K}\boldsymbol{X}$, and (13) can be converted to (10). This completes the proof.

3.2 Control Torque Allocation Scheme Design

The controller spacecraft calculates the control signal $\boldsymbol{u}(t)$ which can stable the combination according to the scheme in the previous section, and then transmits it to the actuator spacecraft. Based on the distributed allocation scheme in this section, the actuator spacecraft will get the control torque they need to generate to stabilize the combination together.

It is assumed that the direction of the control torque $\boldsymbol{u}_i(t)$ allocated to the ith actuator spacecraft is consistent with the direction of the control signal $\boldsymbol{u}(t)$, that is,

$$\boldsymbol{u}_i(t) = \tau_i \boldsymbol{u}(t), \quad i = 1, 2, \ldots n. \tag{14}$$

where $\tau_i \in (0, 1)$ denotes the allocation coefficient and $\sum_{i=1}^{n} \tau_i = 1$.

The working state matrix of the reaction wheel of actuator spacecraft is defined as

$$\boldsymbol{D} = \mathrm{diag}(d_1, d_2, d_3, \ldots d_n) \tag{15}$$

$d_i \in (0, 1)$, $i = 1, 2, 3, \ldots n$ denotes the state factor. Moreover, there may be potential faults in the reaction wheel of each actuator spacecraft, so the effectiveness matrix is introduced and defined as

$$\boldsymbol{G} = \mathrm{diag}(g_1, g_2, g_3, \ldots g_n) \tag{16}$$

where $g_i \in (0, 1)$, $i = 1, 2, 3, \ldots n$ is positively related to the effectiveness of the reaction wheel.

Similar to that described in Ref. [6], the allocation of the control torque can be described as an optimization problem.

$$\begin{array}{ll} \min & \boldsymbol{\tau}^{\mathrm{T}} \boldsymbol{D} \boldsymbol{G} \boldsymbol{\tau} \\ s.t. & \boldsymbol{\alpha} \boldsymbol{\tau} = 1 \\ for & \boldsymbol{\tau} \end{array} \tag{17}$$

where $\boldsymbol{\tau} = [\tau_1,\ \tau_2,\ \ldots\ \tau_n]^{\mathrm{T}}$, $\boldsymbol{\alpha} = \mathbf{1}_{1\times n}$.

The optimal solution of the above weighted least squares problem is [19]

$$\boldsymbol{\tau}^* = \left[l_1^{-1}, l_2^{-1}, l_3^{-1}, \ldots l_n^{-1}\right]^{\mathrm{T}} / \sum_{i=1}^{n} l_i^{-1} \tag{18}$$

where $l_i = d_i g_i,\ i = 1, 2, 3, \ldots n$.

From the form of the optimal solution, it can be seen that the optimal allocation coefficient of each actuator spacecraft is coupled with the state information and actuator effectiveness information of all other spacecraft in the cluster. However, each spacecraft can only communicate directly with its neighbor spacecraft, so a distributed allocation strategy is proposed.

$$\dot{\tau}_i(t) = \sum_{j\in\mathcal{N}(i)} \left(l_j \tau_j(t) - l_i \tau_i(t)\right), \quad i = 1, 2, 3, \ldots n. \tag{19}$$

where $\mathcal{N}(i)$ is the neighbor set of the ith actuator spacecraft.

Then the allocation equation of all actuator spacecraft can be expressed in the following matrix form

$$\dot{\boldsymbol{\tau}}(t) = -\boldsymbol{L}\boldsymbol{D}\boldsymbol{G}\boldsymbol{\tau}(t) \tag{20}$$

$\boldsymbol{L}$ is the Laplacian matrix corresponding to undirected graph $\boldsymbol{\mathcal{G}}$, and $\boldsymbol{\mathcal{G}}$ denotes the topology of the actuator spacecraft. $\boldsymbol{\tau}(t)$ constrained by Eq. (20) will always have the following two properties, and the proof can be found in [6].

(1) $\sum_{i=1}^{n} \tau_i(t) = 1, \forall t \geq 0$, if $\sum_{i=1}^{n} \tau_i(0) = 1$.

(2) $\lim_{t\to\infty} \boldsymbol{\tau}(t) = \boldsymbol{\tau}^* = \left[l_1^{-1}, l_2^{-1}, l_3^{-1}, \ldots l_n^{-1}\right]^{\mathrm{T}} / \sum_{i=1}^{n} l_i^{-1}$.

Remark 2 (1) Ensures that the control torque generated by the actuator spacecraft is always equal to the desired control signal before the allocation coefficient reaches the optimal solution. (2) Shows that the allocation coefficient will reach its optimal solution eventually.

The misalignment of the coordinate frame must be considered in the control torque allocation, so it is necessary to convert the control torque allocated to the ith actuator spacecraft to its body-fixed frame:

$$\boldsymbol{u}_{ai} = [u_{ai1}, u_{ai2}, u_{ai3}, \ldots, u_{aim}]^{\mathrm{T}} = \tilde{\boldsymbol{D}}_i^* \boldsymbol{R}_i^{\mathrm{T}} \boldsymbol{u}_i \tag{21}$$

where $\boldsymbol{u}_{ai}$ denotes the control torque allocated to the ith actuator spacecraft, and $\boldsymbol{R}_i$ is the direction cosine matrix from the body-fixed frame of the ith actuator spacecraft

to the body-fixed frame of the post-capture combination. $\tilde{\boldsymbol{D}}_i^* \in \mathbb{R}^{m\times 3}$ denotes the pseudoinverse of the reaction wheel distribution matrix and m is the number of reaction wheel of each actuator spacecraft.

The working state of reaction wheel reflects its saturation trend. When a reaction wheel tends to be saturated, the corresponding control torque allocated to it should be reduced. Therefore, the working state factor of the ith spacecraft should be negatively related to the control torque allocated to it, as defined below:

$$d_i = \max_{j=1,2,3...m}\left(\text{abs}\left(\frac{L_{ij}(t)}{L_{\max}}\right)\right) \tag{22}$$

where $L_{ij}(t)$ is the angular momentum of the jth reaction wheel of the ith actuator spacecraft. $L_{\max}$ is the saturation angular momentum.

4 Simulation Results

The effectiveness of the Robust H_∞ controller and the control torque allocation scheme are verified by the simulations in this section. $k = 4$, that is, four bending modes are considered in the simulations as shown in Table 1.

The nominal inertia matrix and the coupling matrices are chosen as follows

$$\boldsymbol{J}_n = \begin{bmatrix} 350 & 3 & 4 \\ 3 & 280 & 10 \\ 4 & 10 & 190 \end{bmatrix} \text{kg m}^2$$

$$\tilde{\boldsymbol{\Delta}} = \begin{bmatrix} 6.45637 & -1.25619 & 1.11687 & 1.23637 \\ 1.27814 & 0.91756 & 2.48901 & -0.83674 \\ 2.15629 & -1.67264 & -0.83674 & -1.12503 \end{bmatrix} \sqrt{\text{kg}}\,\text{m}$$

$$\tilde{\boldsymbol{\Delta}}_p = \begin{bmatrix} 2.342552 & -0.422537 & 3.912984 & 7.026176 \end{bmatrix}^{\text{T}} \times 10^{-2}\sqrt{\text{kg}}\,\text{m/s}^2/\text{V}$$

The initial state of the post-capture flexible combination is taken as $\boldsymbol{x}(0) = \begin{bmatrix} \boldsymbol{\Theta}^{\text{T}}(0) & \boldsymbol{\omega}^{\text{T}}(0) & \boldsymbol{q}^{\text{T}}(0) & \tilde{\boldsymbol{\eta}}^{\text{T}}(0) \end{bmatrix}^{\text{T}}$ with $\boldsymbol{\Theta}(0) = \begin{bmatrix} 0.18, & 0.15, & -0.15 \end{bmatrix}^{\text{T}}$ (rad), $\boldsymbol{\omega}(0) = \begin{bmatrix} -0.02, & -0.02, & 0.02 \end{bmatrix}^{\text{T}}$ (rad/s), $\boldsymbol{q}(0) = [0,\ 0,\ 0,\ 0]^{\text{T}}$ and $\tilde{\boldsymbol{\eta}}(0) = [0,\ 0,\ 0,\ 0]^{\text{T}}$.

Table 1 Flexible dynamic parameters

	Natural frequency (rad/s)	Damping
Mode 1	0.7681	0.005607
Mode 2	1.1038	0.008620
Mode 3	1.8733	0.012830
Mode 4	2.5496	0.025160

The difference between the nominal inertia and the actual inertia is assumed as $\Delta \boldsymbol{J} = (0.1 + 0.02\sin(0.11\pi t))\boldsymbol{J}_n$. Take the external disturbance $\boldsymbol{T}_d$ as [20]

$$\boldsymbol{T}_d = 5 \times \left[\sin(0.11\pi t) \quad \cos\left(0.11\pi t + \frac{\pi}{4}\right) \quad \cos\left(0.11\pi t + \frac{\pi}{3}\right)\right]^{\mathrm{T}} \times 10^{-4}\,\mathrm{Nm}$$

The measurement error of the sensor is

$$\boldsymbol{v}(t) = [4\ 5\ 6\ 0.2\ 0.2\ 0.2\ 0.2\ 0.1\ 0.2\ 0.2\ 0.2\ 0.2\ 0.1\ 0.2]^{\mathrm{T}} \times \sin(0.01\pi t) \times 10^{-4}$$

where the units of error corresponding to angle and angular velocity are rad and rad/s.

The feedback coefficient matrices are chosen as

$$\boldsymbol{F}_a = [3.1533 \quad -0.5714 \quad 5.3674 \quad 9.3389]$$
$$\boldsymbol{F}_b = [1.0976 \quad 0.1965 \quad 1.8086 \quad 3.0873]$$

and the other parameters are shown as follows:

$$\boldsymbol{M} = 0.01 \times [8\ 11\ 13\ 15\ 16\ -18\ 8\ 11\ 13\ 15\ 16\ 18\ 8\ 11]^{\mathrm{T}},$$
$$\boldsymbol{F} = \sin(0.11\pi t)$$

$$\boldsymbol{N} = 0.01 \times [1\ 2\ 3\ 4\ 2\ 10\ 1\ 2\ 3\ 4\ 2\ 10\ 1\ 2],$$
$$\boldsymbol{M}_a = 0.1 \times \boldsymbol{1}_{3\times 1}, \quad \boldsymbol{F}_a = \sin\left(0.11\pi t + \frac{\pi}{4}\right)$$

$$\boldsymbol{N}_a = 0.01 \times \boldsymbol{1}_{1\times 14}, \boldsymbol{M}_m = 0.1 \times \boldsymbol{1}_{3\times 1}, \boldsymbol{F}_m = \cos(0.11\pi t), \boldsymbol{N}_m = 0.01 \times \boldsymbol{1}_{1\times 3}$$

$$\overline{\rho} = 0.6, \eta_0 = 0.8083, \xi = 0.002, \xi_a = 0.22, \xi_m = 0.22$$

$$\varepsilon = 0.05, \gamma_0 = 0.65, \lambda_0 = 27$$

Assume that $n = 6$, that is, there are 6 actuator spacecraft. The effectiveness factors are shown in Table 2.

Table 2 Effectiveness factors

	Effectiveness factors g_i
Actuator spacecraft 1	$0.65 + 0.35e^{-0.088t}$
Actuator spacecraft 2	$0.81 + 0.19e^{-0.078t}$
Actuator spacecraft 3	$0.74 + 0.26e^{-0.064t}$
Actuator spacecraft 4	$0.66 + 0.34e^{-0.042t}$
Actuator spacecraft 5	$0.56 + 0.44e^{-0.068t}$
Actuator spacecraft 6	$0.88 + 0.12e^{-0.038t}$

The Euler angles between the body-fixed frame of the ith actuator spacecraft and the body-fixed frame of the post-capture combination are shown in Table 3.

The fault signal $f_d(t)$ is shown in Table 4, and actuator faults $\boldsymbol{f}(t) = \left[0.003 f_d(t)\ 0.004 f_d(t)\ 0.005 f_d(t)\right]^{\mathrm{T}}$.

The communication topology of the controller and actuator spacecraft is shown in Fig. 1. "C" is the controller spacecraft which is connected to the actuator spacecraft 2, 4 and 6, and other numbers also denote the actuator spacecraft.

The Laplacian matrix $\boldsymbol{L}$ corresponding to Fig. 1 is

$$\boldsymbol{L} = \begin{bmatrix} 2 & -1 & -1 & 0 & 0 & 0 \\ -1 & 3 & -1 & -1 & 0 & 0 \\ -1 & -1 & 4 & 0 & -1 & -1 \\ 0 & -1 & 0 & 2 & -1 & 0 \\ 0 & 0 & -1 & -1 & 3 & -1 \\ 0 & 0 & -1 & 0 & -1 & 2 \end{bmatrix}$$

Table 3 Euler angles

	Euler angles (rad)
Actuator spacecraft 1	$\pi/180 \times [8.60, 2.10, 9.66]^{\mathrm{T}}$
Actuator spacecraft 2	$\pi/180 \times [-0.31, -2.34, 6.72]^{\mathrm{T}}$
Actuator spacecraft 3	$\pi/180 \times [-9.22, 7.44, 2.88]^{\mathrm{T}}$
Actuator spacecraft 4	$\pi/180 \times [-6.99, 8.36, 9.13]^{\mathrm{T}}$
Actuator spacecraft 5	$-\pi/180 \times [10.01, 2.33, 5.55]^{\mathrm{T}}$
Actuator spacecraft 6	$\pi/180 \times [0.88, -7.65, -8.88]^{\mathrm{T}}$

Table 4 $f_d(t)$

t (s)	[0, 5]	(5, 35]	(35, 70]	(70.0, 120.0]	(120.0, 150.0]
$f_d(t)$ (Nm)	0	$\cos(0.1\pi t)$	1.0	1	0

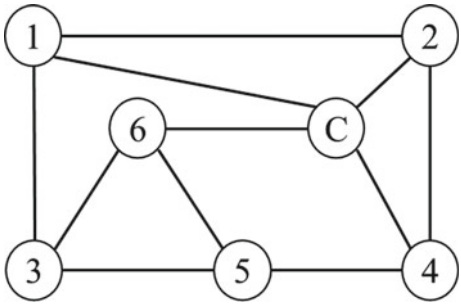

Fig. 1 Communication topology

Assume that each actuator spacecraft is equipped with four reaction wheels and the distribution matrix is

$$\boldsymbol{D}_i = \begin{bmatrix} -\frac{1}{\sqrt{3}} & -\frac{1}{\sqrt{3}} & \frac{1}{\sqrt{3}} & \frac{1}{\sqrt{3}} \\ \frac{1}{\sqrt{3}} & -\frac{1}{\sqrt{3}} & -\frac{1}{\sqrt{3}} & \frac{1}{\sqrt{3}} \\ \frac{1}{\sqrt{3}} & \frac{1}{\sqrt{3}} & \frac{1}{\sqrt{3}} & \frac{1}{\sqrt{3}} \end{bmatrix}, \quad i = 1, 2, 3, 4.$$

The initial momentum of every reaction wheel of each actuator spacecraft is shown in Table 5. In addition, the saturated momentum is $L_{\max} = 20\,(\mathrm{kg\,m^2})/\mathrm{s}$.

Substitute the relevant parameters into Theorem 1, and solve the optimization to obtain the controller gain $\boldsymbol{K}$ as

$$\boldsymbol{K} = \begin{bmatrix} -10.9179 & -5.3450 & 6.2522 & -176.6787 & -42.1617 & -35.7863 & 2.4703 \\ -4.7984 & -8.9688 & 2.6129 & -86.0076 & -181.6544 & 12.5528 & 14.3448 \\ -4.0037 & -1.1768 & -27.5459 & -62.9165 & -43.4558 & -73.9154 & 3.8657 \\ -17.3200 & 10.8289 & 1.8054 & 7.4823 & -18.4810 & -3.8505 & -2.2469 \\ 32.1448 & 10.8867 & -9.5563 & 11.0959 & 10.7721 & 17.3920 & 12.7571 \\ 8.4216 & 11.2888 & 1.1193 & 6.0801 & -6.8043 & -6.9163 & -6.4342 \end{bmatrix}$$

and the minimum value of the optimized variable is $\gamma_{\min}^2 = 1.1112$.

Apply the controller to the closed-loop control system for simulation, and the total control torque generated by actuator spacecraft is shown in Fig. 2, and the allocation error is defined as the difference between the desired control torque signal and the total control torque generated by the actuator spacecraft, which is plotted in Fig. 3. Figure 2 shows that the control torque is always limited to $\pm$ 0.5 Nm, which meets the control objective. The torque allocation error is always less than 2×10^{-15} Nm, which shows the success of the allocation scheme. The high-precision control torque allocation scheme can also be used in conjunction with other controller schemes.

The convergence time of attitude angle and angular velocity is 32.2 s and 16.4 s respectively, and their steady-state control accuracy can reach 3×10^{-5} rad and 1×10^{-5} rad/s. The first four modes can be stabilized within 18.5 s and finally suppressed within 2×10^{-5}. In addition, the total energy consumption and vibration

Table 5 Initial momentum

	Initial momentum $L_{ij}(0)$ $((\mathrm{kg\,m^2})/\mathrm{s})$
Actuator spacecraft 1	$[-5.20, 18.50, 35.55, 24.00]^{\mathrm{T}} \times 10^{-2} L_{\max}$
Actuator spacecraft 2	$[26.70, 25.74, -10.21, 12.36]^{\mathrm{T}} \times 10^{-2} L_{\max}$
Actuator spacecraft 3	$[-35.34, -28.56, -14.52, 34.12]^{\mathrm{T}} \times 10^{-2} L_{\max}$
Actuator spacecraft 4	$[9.44, -33.33, 26.26, 35.55]^{\mathrm{T}} \times 10^{-2} L_{\max}$
Actuator spacecraft 5	$[-29.38, 21.45, 30.02, 12.58]^{\mathrm{T}} \times 10^{-2} L_{\max}$
Actuator spacecraft 6	$[1.88, -9.02, -4.08, 5.66]^{\mathrm{T}} \times 10^{-2} L_{\max}$

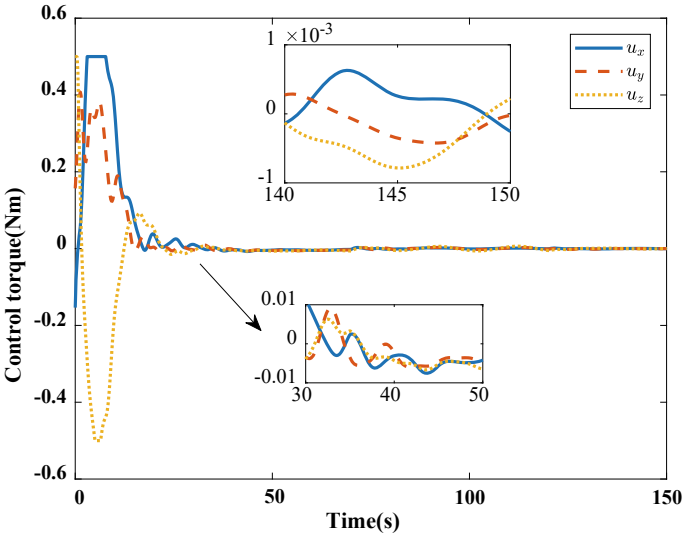

Fig. 2 The total control torque

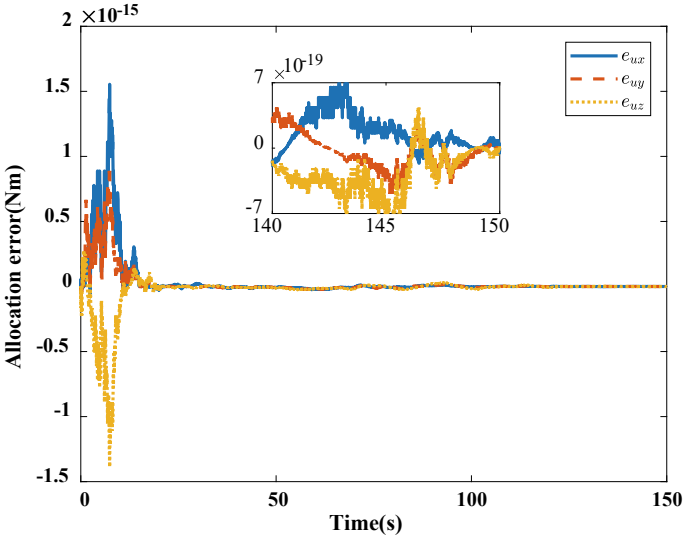

Fig. 3 Allocation error

energy are defined as $E_0 = \frac{1}{2}\int_0^{t_0} \|\boldsymbol{u}\| dt$ and $E_v = \int_0^{t_0} \left(\dot{\tilde{\boldsymbol{\eta}}}^{\mathrm{T}} \dot{\tilde{\boldsymbol{\eta}}} + \tilde{\boldsymbol{\eta}}^{\mathrm{T}} \tilde{\boldsymbol{K}} \tilde{\boldsymbol{\eta}}\right) dt$ with t_0 denoting the simulation time. It can be clearly seen that the vibration energy of post-capture flexible combination is very small, indicating that the elastic vibration of flexible appendages is well suppressed, "which is consistent with Fig. 6".

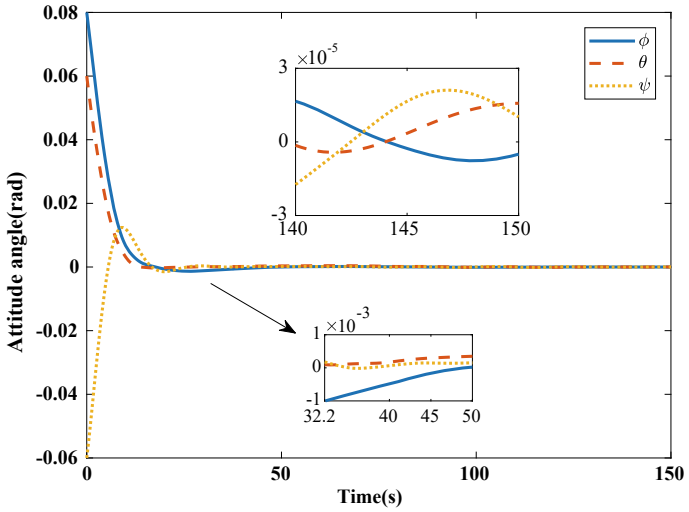

Fig. 4 The curve of attitude angle

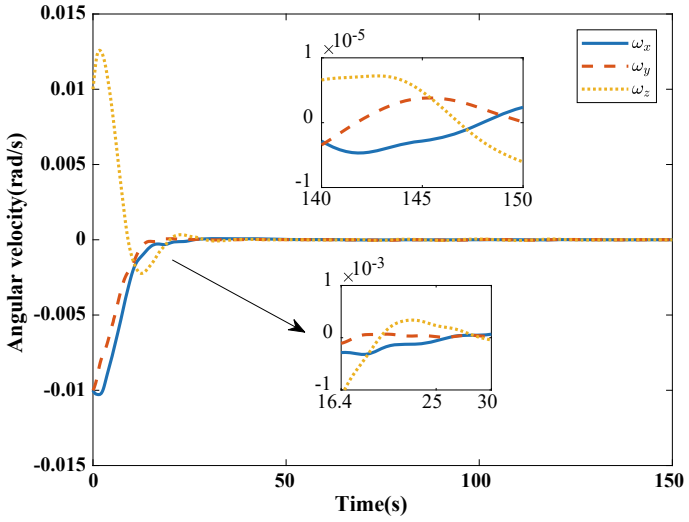

Fig. 5 The curve of angular velocity

The angular momentum curves of the four reaction wheels of the first three actuators spacecraft are drawn in Fig. 8, and the last three are drawn in Fig. 9. The two pictures show that during the whole torque allocation process, all reaction wheels are not saturated, and their maximum angular momentum is less than $L_{\max} = 20\,(\mathrm{kg\,m^2})/\mathrm{s}$, which shows that the dynamic torque allocation strategy is successful.

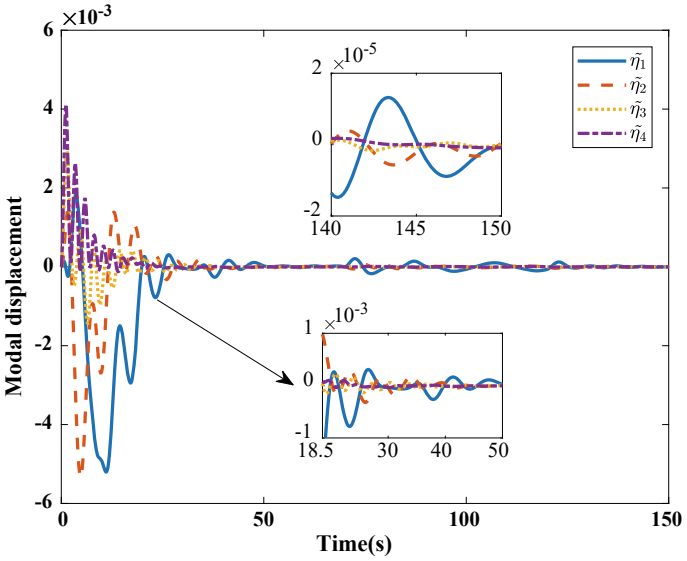

Fig. 6 The curve of modal displacement

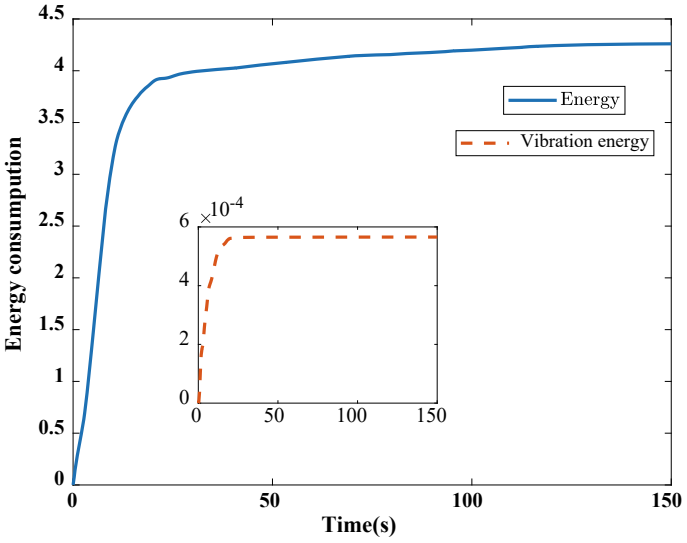

Fig. 7 The curve of energy

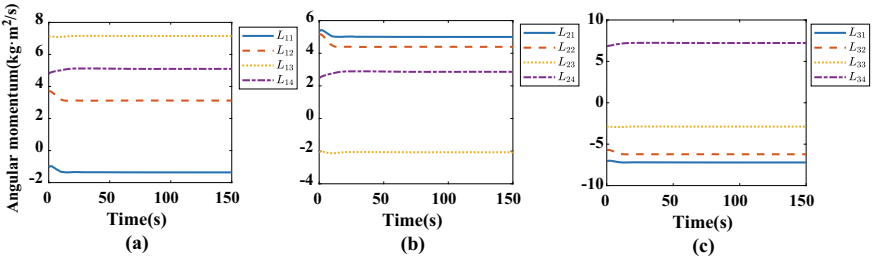

Fig. 8 The angular momentum of the 1–3rd actuator spacecraft

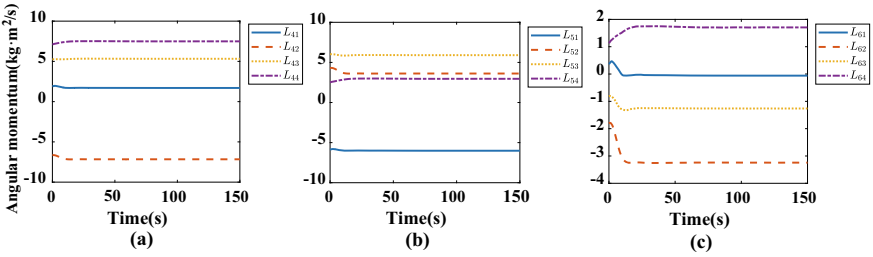

Fig. 9 The angular momentum of the 4–6th actuator spacecraft

5 Conclusions

In this paper, a robust H_∞ control scheme is proposed for the cluster takeover of non-cooperative flexible spacecraft, which is preset on the controller spacecraft in the cluster. The controller spacecraft is responsible for calculating the control signal that can stabilize the post-capture flexible combination, while the actuator spacecraft implement the allocated control torque based on the torque allocation strategy. The control scheme provides a feasible solution for realizing the attitude stabilization and vibration suppression of the flexible combination simultaneously, while the torque allocation scheme restores the desired control signal scheme with high precision.

Funding Statement This work was supported in part by the National Natural Science Foundation of China under Grants U21B6001, 11972026 and U2013206, in part by Science and Technology on Space Intelligent Control Laboratory under Grant 2021-JCJQ-LB-010-07, and in part by Key Research and Development Program of Shaanxi under Grant 2023-YBGY-384.

References

1. Li, S., She, Y.: Recent advances in contact dynamics and post-capture control for combined spacecraft. Prog. Aerosp. Sci. **120**, 100678 (2021)
2. Chai, Y., Luo, J., Han, N., et al.: Robust event-triggered game-based attitude control for on-orbit assembly. Aerosp. Sci. Technol. **103**, 105894 (2020)
3. Dai, H., Cao, X., Jing, X., et al.: Bio-inspired anti-impact manipulator for capturing non-cooperative spacecraft: theory and experiment. Mech. Syst. Signal Process. **142**, 106785 (2020)
4. Liu, C., Yue, X., Yang, Z.: Are nonfragile controllers always better than fragile controllers in attitude control performance of post-capture flexible spacecraft. Aerosp. Sci. Technol. **118**, 107053 (2021)
5. Ning, K., Wu, B., Xu, C.: Event-triggered adaptive fuzzy attitude takeover control of spacecraft. Adv. Space Res. **67**(6), 1761–1772 (2021)
6. Chang, H., Huang, P., Zhang, Y., et al.: Distributed control allocation for spacecraft attitude takeover control via cellular space robot. J. Guid. Control Dyn. **41**(11), 2499–2506 (2018)
7. Xu, Y., Han, T., Cai, K., et al.: A distributed algorithm for resource allocation over dynamic digraphs. IEEE Trans. Signal Process. **65**(10), 2600–2612 (2017)
8. Liu, W., Geng, Y., Wu, B., et al.: Distributed constrained control allocation for cellularized spacecraft attitude control system. J. Guid. Control Dyn. **45**(2), 385–393 (2022)
9. Lang, X., de Ruiter, A.: A control allocation scheme for spacecraft attitude stabilization based on distributed average consensus. Aerosp. Sci. Technol. **106**, 106173 (2020)
10. Yang, Z., Liu, C., Yue, X.: NI-based static output feedback control for attitude stabilization of post-capture flexible spacecraft. Adv. Space Res. (2022)
11. Liu, C., Shi, K., Yue, X., et al.: Inertia-free saturated output feedback attitude stabilization for uncertain spacecraft. Int. J. Robust Nonlinear Control **30**(13), 5101–5121 (2020)
12. Di Gennaro, S.: Output stabilization of flexible spacecraft with active vibration suppression. IEEE Trans. Aerosp. Electron. Syst. **39**(3), 747–759 (2003)
13. Sidi, M.J.: Spacecraft Dynamics and Control: A Practical Engineering Approach. Cambridge University Press (1997)
14. Liu, C., Shi, K., Sun, Z.: Robust H_∞ controller design for attitude stabilization of flexible spacecraft with input constraints. Adv. Space Res. **63**(5), 1498–1522 (2019)
15. Liu, C., Yue, X., Shi, K., et al.: Inertia-free attitude stabilization for flexible spacecraft with active vibration suppression. Int. J. Robust Nonlinear Control **29**(18), 6311–6336 (2019)
16. Lyu, B., Yue, X., Liu, C.: Constrained multi-observer-based fault-tolerant disturbance-rejection control for rigid spacecraft. Int. J. Robust Nonlinear Control **32**(14), 8102–8133 (2022)
17. Boyd, S.P., Ghaoui, L.E., Balakrishnan, V.: Linear Matrix Inequality in System and Control Theory. SIAM, Philadelphia (1994)
18. Liu, C., Yue, X., Zhang, J., et al.: Active disturbance rejection control for delayed electromagnetic docking of spacecraft in elliptical orbits. IEEE Trans. Aerosp. Electron. Syst. (2021)
19. Shi, M., Wu, B., Wang, D.: Neural-network-based adaptive quantized attitude takeover control of spacecraft by using cellular satellites. Adv. Space Res. **70**(7), 1965–1978 (2022)
20. Yang, C.D., Sun, Y.P.: Mixed H_2/H_∞ state-feedback design for microsatellite attitude control. Control Eng. Pract. **10**(9), 951–970 (2002)